Journal of
Manufacturing and Materials Processing

MDPI

Article

Experimental Investigation on the Cutting of Additively Manufactured Ti6Al4V with Wire-EDM and the Analytical Modelling of Cutting Speed and Surface Roughness

Manuela Galati *, Paolo Antonioni, Flaviana Calignano and Eleonora Atzeni

Department of Management and Production Engineering, Politecnico di Torino, Corso Duca degli Abruzzi 24, 10129 Torino, Italy
* Correspondence: manuela.galati@polito.it

Abstract: Additive manufacturing (AM) technologies for metallic materials allow for the manufacturing of high-performance components optimised in weight, geometry, and mechanical properties. However, several post-processing operations are needed after production, including removing parts from the build platform. This operation is essential and must be performed rapidly, precisely, and with a good surface finishing. This work presents an experimental investigation of the wire electric discharge machining (W-EDM) process of Ti6Al4V specimens produced by AM technologies. The influence of cutting parameters is analysed compared to the material produced by conventional technology. Models of cutting speed and surface roughness obtained by a W-EDM are inferred from the collected data. Remarkably, the results show that the manufacturing process used to produce the components plays a crucial role in defining the final surface roughness and the most significant parameters affecting the machining performance.

Keywords: electron beam powder bed fusion; laser powder bed fusion; wire electrical discharge machining; surface roughness; cutting speed

Citation: Galati, M.; Antonioni, P.; Calignano, F.; Atzeni, E. Experimental Investigation on the Cutting of Additively Manufactured Ti6Al4V with Wire-EDM and the Analytical Modelling of Cutting Speed and Surface Roughness. *J. Manuf. Mater. Process.* **2023**, *7*, 69. https://doi.org/10.3390/jmmp7020069

Academic Editor: Muhammad Pervej Jahan

Received: 14 February 2023
Revised: 10 March 2023
Accepted: 13 March 2023
Published: 16 March 2023

1. Introduction

Wire-electric discharge machining (W-EDM) is an electro-thermal non-conventional machining process used to machine hard-to-cut materials. An electrical circuit is created between two electrodes, the workpiece and the wire tool, separated by a dielectric fluid, typically deionised water. The process consists of recurring sparks when an electrical voltage is applied between the workpiece and the wire [1]. Where the discharge takes place, the material is removed by evaporation or ejection in the liquid phase. The removed material cools down rapidly because of the presence of deionised water and solidifies into small spherical particles, called debris, which are flushed away by the dielectric fluid [2]. On the surface of the workpiece, small craters can be observed where the material has been removed. The presence of such craters defines the technological signature left by W-EDM machining. Because of the absence of mechanical contact between the two electrodes, no cutting tool forces are created while machining [2]. Therefore, only the workpiece electrical and thermal properties are relevant for the process [3]. This aspect allows for its use with difficult-to-cut materials [4] and represents one of the most significant advantages of W-EDM over other cutting machining processes.

Commonly, the absence of both wire breakage and spark indicates stable process conditions [5], and quantitative indicators such as the material removal rate (MRR), the cutting speed (V_c), and the surface roughness of the machined workpiece (SR) are used to measure the process characteristics under specific processing parameters. As an example, combination of high pulse on-time (t_{on}) and discharge current (I) make the process faster, but is detrimental to the surface roughness, the kerf width (KW), and the wire wear ratio (WWR) [6–14]. Higher pulse off-time (t_{off}) values lower the MRR and the cutting speed,

but are beneficial for the surface roughness [15–18]. However, in some cases, the surface roughness worsens over a certain t_{off} value [19,20]. Higher servo voltage (SV) values increase KW and enhance the surface finishing, but reduce the MRR, the cutting speed, and the WWR [6,13,18,21–28]. Higher open-circuit voltage (V) causes higher MRR, cutting speed, KW, and surface roughness [29]. Other factors, such as wire feed rate (WF), wire tension (WT), and dielectric pressure (DP), or dielectric flow rate, less significantly affect the W-EDM performance [27–32]. The workpiece thickness has been scarcely investigated, although it has been demonstrated to affect the process results [31,33]. A cross-comparison among the literature studies revealed some contrasting findings. For example, some work [10,17,21] demonstrated that higher t_{off} values could reduce the surface roughness, but the opposite result has been shown in refs. [19,20]. In addition, material processing technology has never been considered as a determining factor.

However, using different processing technologies may affect the W-EDM performance, especially in the case of additive manufacturing (AM), which can process conventional metallic materials using a completely new approach. On the other hand, the advent of AM for metallic components led to significant W-EDM development and market growth. In fact, W-EDM is the preferable option for removing additive manufactured parts from the build platform onto which they were produced. However, few studies have investigated the working conditions during the W-EDM of AM parts [34,35], and these have focused only on specimens of AlSi10Mg and produced by laser powder bed fusion (PBF-LB) based AM systems [34,35].

This work investigates the performance of W-EDM when cutting the same nominal material, Ti6Al4V, produced with different processing technologies: casting, PBF-LB, and electron beam powder bed fusion (PBF-EB). The quality of the cut surface is evaluated using the surface roughness index, while the process efficiency is evaluated using the cutting speed. The effects of the process parameters, including the workpiece thickness, on these indexes are analysed using descriptive and inferential statistical tools, and regression models are inferred from the collected data.

2. Materials and Methods

2.1. Design of the Artefacts and Production

The artefact consists of three parallelepipedal sections of dimensions: 10 mm × 10 mm, 20 mm × 20 mm, and 30 mm × 30 mm, respectively, and the thickness of each section is 15 mm, corresponding to the cutting length. A replica of the artefact has been produced using an EOSINT M270 Dual Mode machine, an PBF-LB system, and an Arcam A2X, an PBF-EB system. For the PBF-LB and PBF-EB processes, the same nominal chemical composition of Ti6Al4V powder was used. The average particle size was 45 µm and 75 µm for the EOSINT and Arcam systems, respectively.

Figure 1 depicts the artefact geometry with the build direction (z-axis), the used machines, and the as-built artefacts. The process parameters are collected in Tables 1 and 2. After the production, the replicas were cleaned from loose powder. In addition, the PBF-LB artefact has been subjected to stress-relieving treatment (in a furnace at 800 °C for 2 h). For the casting samples analysis, three commercial Ti6Al4V plates that copy the three parallelepipedal sections of the AMed artefact have been used for the analysis.

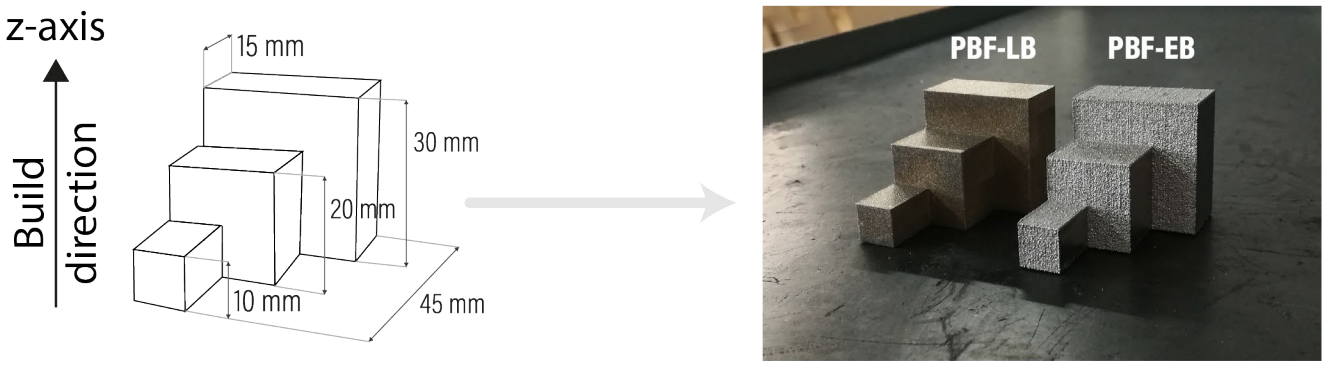

Figure 1. Workpiece geometry and production.

Table 1. PBF-LB process parameters [36].

	Laser Power [W]	Scan Speed [mm/s]	Hatching Distance [mm]	Layer Thickness [µm]	Laser Spot Size [mm]
Hatch (Core)	170	1250	0.10	30	0.10
Hatch (Skin)	150	1000	0.10	30	0.10
Contour	120	1250	-	-	0.10

Table 2. EB-BPF process parameters [37].

	Scan Speed [mm/s]	Focus Offset [mA]	Beam Current [mA]	Number of Contours	Hatch Contours [mm]	Line Offset [mm]
Hatch	45	25	20	-	-	0.2
Contour	850	6	5	3	0.290	0.200

2.2. Design of Experiment (DoE)

The machining was performed using a BAOMA DK7732 machine, a 4-axes high-speed feed W-EDM machine supplied by Suzhou Baoma Numerical Control Equipment Co. Ltd., Suzhou, China. The machine is equipped with a CNC pulse generator, a dielectric fluid supply system, a working table, a wire electrode drive and supply system, and a separate controller through which it is possible to adjust or modify the machine and the process parameters. A molybdenum wire electrode with a 0.18 mm diameter is reciprocally fed and used in the working area at high speed to limit the wire wear.

In light of the literature analysis, the selected parameters were: discharge current (I), pulse on-time (t_{on}), pulse off-time (t_{off}), and workpiece thickness. From the literature, it is well known that I and t_{on} should be selected according to the workpiece layer thickness.

However, because standard W-EDM machine does not include adaptive control and additively manufactured components often include variable thicknesses, the evaluation of the effect of I and t_{on} together with the thickness on W-EDM performance indexes were considered extremely important.

The W-EDM system used for the experiments does not allow for the control of t_{off} directly and independently from t_{on}. The relationship between the actual value of t_{off} and t_{on} is presented in Equation (1), in which t_{off}* is a multiplicative coefficient that can vary from 1 to 30.

$$t_{off} = t_{on} \times (t_{off}* + 1) \quad (1)$$

For this reason, the investigation of t_{off} was replaced by selecting three levels of duty cycle (DC) (Table 3). DC is defined as the percentage of the active phase duration (t_{on}) with respect to the total cycle time (Equation (2)) [38].

$$DC\ [\%] = \left(\frac{t_{on}}{t_{on}+t_{off}}\right) \times 100 \quad (2)$$

Table 3. Investigated process parameters and their levels.

Level	Low	Medium	High
I [A]	2	3	4
t_{on} [µs]	10	20	30
DC [%]	5.88	8.33	14.29
Thickness [mm]	10	20	30

Consequently, t_{off}* was selected accordingly to maintain the DC constant (Table 3). A full factorial designed plan was implemented, considering three levels for each process parameter (factor) for a total of 81 experimental runs.

The dielectric used was a solution made of deionised water and an additive provided by the machine producer, whose commercial name is BM-4. The open circuit voltage was kept to 80 V during all experiments, and the wire feed speed was kept at the maximum level, corresponding to 11 m/s. All experimental trials were randomised to reduce the systematic effects of uncontrolled variables, such as wire wear. The runs were repeated using the same process conditions for each artefact replica produced by different technologies.

2.3. Performance Indexes Calculation

The total length of the cut was 15 mm. During the experimental runs, the time required to perform the cut was collected, and the cutting speed, V_c, was calculated according to Equation (3).

$$V_c\ [mm/min] = \text{Cut length } [mm]/\text{Cutting time } [min] \quad (3)$$

The adopted procedure for the cutting consisted of the following steps:

1. Workpiece positioning and clamping on W-EDM machine guides;
2. Wire electrode positioning and axis resetting;
3. Setting process parameters and wire linear path;
4. Machining the workpiece from the thinner to the thicker thickness;
5. Measuring the time necessary to perform the cut for each thickness.

After the machining; the arithmetical mean roughness value, Ra, of the resulting surface was measured according to ISO 4288 [39], using an RTP 80 profilometer produced by SM Metrology Systems. Based on previous authors' works [37,40], data were collected using a cut-off length of 0.8 mm and a sample length of 4 mm. Six measurements of the surface roughness were acquired for each surface (Figure 2b), for a total of 486 roughness measurements per DoE: three along the cutting direction (*x*-axis in Figure 2a) and three orthogonally to the previous one (*y*-axis in Figure 2a). The Ra value (Figure 2b) was calculated using the relationship reported in Equation (4)

$$Ra\ [\mu m] = \frac{1}{l}\int_0^l |f(x)|dx \quad (4)$$

where f(x) is the roughness profile, and l is the sample length. For each direction and sample thickness, the average values of Ra in each direction were calculated by averaging the three Ra measured values.

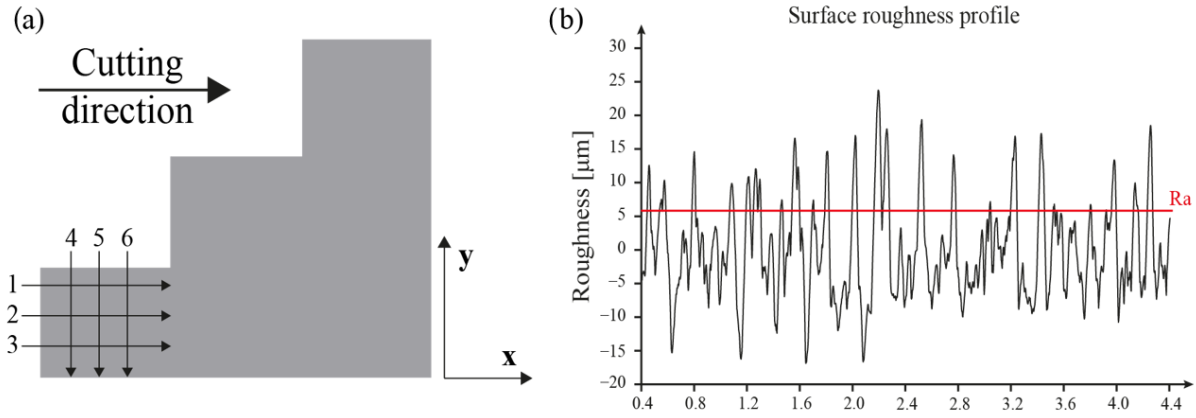

Figure 2. (**a**) Measurement directions for the evaluation of bulk workpiece surface roughness (Ra); (**b**) surface roughness profile and Ra value.

The cutting speed (V_c) and surface roughness (Ra) collected along two orthogonal directions were analysed using the Minitab 19 environment. The statistical question investigates whether the manufacturing process affected V_c and Ra and determines the variables contributing to V_c and Ra variations. Regarding Ra, the study of the effects of the manufacturing process and cutting parameters were analysed separately in the two measurement directions, respectively, for Ra_x and Ra_y. Initially, the data were grouped according to the workpiece production process, and then the data were analysed to detect the effect of the investigated factors and their interaction with the V_c and Ra values.

The surfaces of the samples after the cut were also observed with a stereomicroscope, an optical microscope, and SEM.

3. Results and Discussion

Figure 3 compares the surface texture obtained under the same processing condition for each production technology. The surface texture is clearly different among the manufacturing technologies. The surface belonging to the casted sample (Figure 3a) is characterised by small and almost uniform craters. Both the surfaces belonging to the pieces produced by PBF-EB (Figure 3b) and L-PBF (Figure 3c) are characterised by a wave pattern in the wire advancement direction, which could be mainly caused by the periodic inversion of the wire rotation. For the casted sample (Figure 3a,d), the dimensions of the craters are smaller compared to the ones on PBF-EB (Figure 3b,e) and PBF-LB (Figure 3c,f).

In addition, the surfaces show a certain quantity of spherical debris (examples are indicated with white arrows), which vary in size and concentration according to the material processing technology. They appear to be smaller in dimensions and number on casted sample surfaces than on PBF-LB or PBF-EB surfaces, where a large amount of the particles is attached to the surface on which the wire inversions took place. This effect is more evident for the PBF-LB sample, in which the craters on the surface are more prominent than in other processes. In fact, the average size of these debris is 14.75 ± 4.02 µm for PBF-LB, 17.73 ± 4.87 µm for PBF-EB, and 12.83 ± 2.13 µm for casting.

The white spherical particles attached to the sample surface (examples are indicated with red arrows) are residual from the electrode, in this case, Molybdenum. The average size of these residual is 3.69 ± 0.69 µm for PBF-LB, 3.30 ± 0.55 µm for PBF-EB, and 3.32 ± 0.72 µm for casting. No significant difference has been detected among the processes.

From the SEM images of the workpiece surface (Figure 3d–f), it is also possible to obtain an indication regarding the craters typically produced by the W-EDM process (examples are indicated by yellow arrows).

Some superficial cracks are also visible, which are caused by high temperature and subsequent rapid cooling.

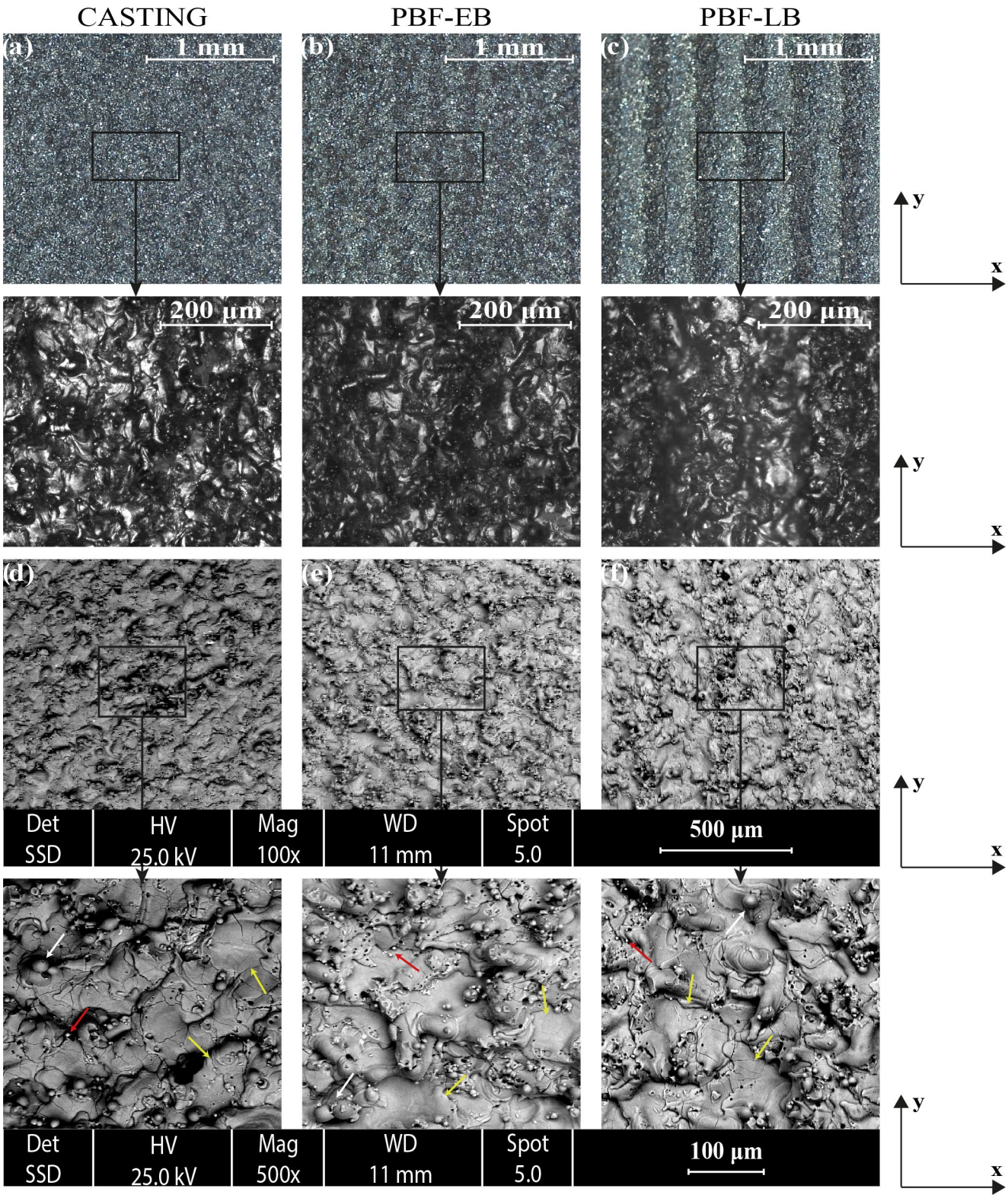

Figure 3. Surface textures observed with (**a**–**c**) microscope and (**d**–**f**) SEM on samples produced by (**a**,**d**) casting, (**b**,**e**) PBF-EB, and (**c**,**f**) PBF-LB, machined with the same set of process parameters (t_{on} = 10 s, DC = 8.33%, I = 3 A, workpiece thickness = 20 mm). White arrows indicate examples of spherical debris; red arrows indicate examples of residuals from the wire, while yellow arrows provide an example of craters produced on the workpiece surface by the W-EDM process. The *x*-axis is parallel to the cut direction.

As an example, analysing the surfaces in Figure 3, the roughness of the surfaces is described by the root mean square value within the cut area, Sq. In this case, the measured value of the entire surface was 8.17 µm for PBF-LB, 4.41 µm for PBF-EB, and 4.60 µm for casting. A strong difference between PBF-LB and the other processes is evident. However, the surfaces show grossly different spatial features, which are revealed by measuring the Ra_x and Ra_y (Table 4). Moreover, the more the pattern is evident, as in the case of PBF-LB (Figure 3c), the higher the measured surface roughness is, especially in the wire advancement direction (Ra_x), as can be observed in Table 4. The pattern can be also noted in the topographies reported in Figure 4.

Table 4. Surface roughness average and standard deviation values for each direction and material manufacturing technology.

Process	Ra_x (Std. Deviation) [µm]	Ra_y (Std. Deviation) [µm]	V_c (Std. Deviation) [µm]
CASTING	6.88 (1.33)	6.62 (1.39)	1.30 (0.77)
PBF-EB	8.63 (1.72)	7.93 (1.68)	1.32 (0.76)
PBF-LB	9.99 (2.96)	8.55 (2.10)	1.35 (0.74)

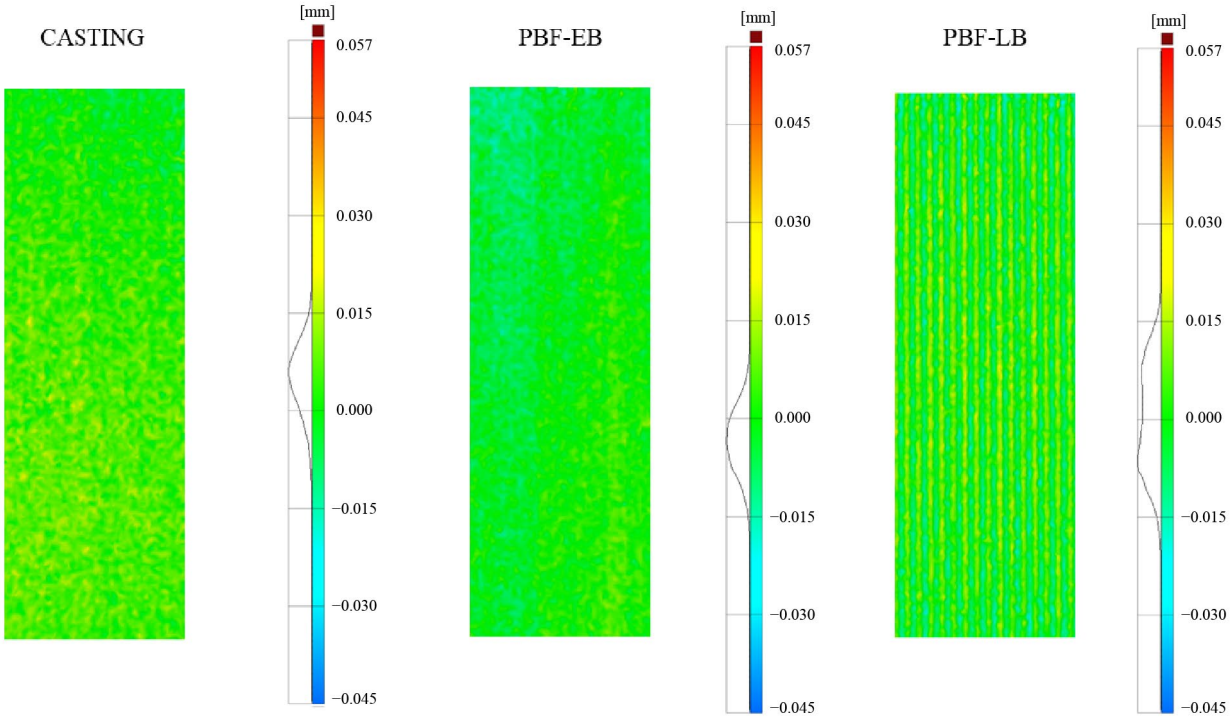

Figure 4. Surface topography images for samples produced with casting, PBF-EB, and PBF-LB, machined with the same process parameters (t_{on} = 10 s, DC = 8.33%, I = 3 A, workpiece thickness = 20 mm).

This point was confirmed by an ANOVA analysis (Table 5), which highlighted, with a risk level of 0.05, a significant difference between the surface roughness measured in the two directions for PBF-EB and PBF-LB. In addition to the above conclusion, the more the pattern is evident, the more significant the difference between the two values. Since the surface roughness is always higher in the wire advancement direction (Table 4), Ra_x represents the most critical index for describing the surface finish of the machined surface. For this reason, only Ra_x is discussed. For completeness, the results concerning Ra_y are presented in Appendix A.

Table 5. ANOVA results of surface roughness in the two directions.

	Source of Variation	DoF	Variance	F-Ratio	F-Max
CASTING	Examined factor	1	2.809	1.52	3.90
	Error	160	1.849		
	Total	161			
PBF-EB	Examined factor	1	19.806	6.86	3.90
	Error	160	2.889		
	Total	161			
PBF-LB	Examined factor	1	84.216	12.77	3.90
	Error	160	6.594		
	Total	161			

As can be observed in Table 4, the cut surface of samples manufactured by the PBF-LB process are more dispersed, and the surfaces are rougher than the corresponding PBF-EB and casted counterparts. In particular, the average value of Ra_x for the casted workpiece (6.88 µm) was significantly lower than those registered for their PBF-LB and PBF-EB counterparts (9.99 µm and 8.63 µm, respectively). This result indicates the presence of a systematic effect of the material manufacturing technology on the surface roughness. This result is also confirmed by the analysis of variance (ANOVA) in Table 6, which also showed no significant differences for the V_c values using various sample production methods.

Table 6. ANOVA results for the effect of production technology over cutting speed (V_c) and surface roughness Ra_x.

	Source of Variation	DoF	Variance	F-Ratio	F-Max
V_c	Examined factor	2	3.80×10^{-2}	0.07	3.03
	Random errors	240	5.75×10^{-1}		
	Total	242			
Ra_x	Examined factor	2	1.97×10^{2}	43.74	3.03
	Random errors	240	4.51		
	Total	242			

Figure 5 shows the main effects of process parameters on V_c and Ra_x for each technology. In agreement with the previous findings, no significant differences among the technologies can be noticed in the effect of the investigated factors on V_c. An increasing discharge current value causes an increase in the discharge energy and thus, the cutting speed or MRR, in agreement with refs. [7,10,12,29]. A thicker cut determines a lower value of cutting speed. This could be explained by the more considerable amount of material to be removed with the same discharge energy when increasing the thickness, thus causing a cutting speed reduction. Compared to DC, even if t_{on} determines the discharge duration and the productive phase, it does not significantly affect the cutting speed. This could be explained by the multiplicative relationship between the t_{off} and t_{on}, valid for high-speed W-EDM, presented in Equation (2). This relationship implies the presence of high unproductive times (t_{off}) that are always larger than the productive examples. Consequently, DC is low and limits the machine productivity. For this reason, if an increasing erosion rate does not compensate for an increased t_{off} during the productive phase, the unproductive phase becomes the main factor affecting the cutting speed and thus, the process productivity. The effect of t_{off} agrees with that noted in refs. [15,18].

Regarding surface roughness, contrasting findings can be detected and are peculiar to the material manufacturing process. For the PBF-LB, the increasing discharge current seems to have a quadratic effect on the surface roughness, with a maximum value at 3 A. For PBF-EB instead, only slight Ra_x variations were observed for currents between 3 A and 4 A. According to Equation (3), an increase in DC and a corresponding reduction of t_{off} produces smoother surfaces in the case of parts produced by PBF-LB. Instead, for parts manufactured by PBF-EB, an increase in DC and thus, a reduction of t_{off}, increases the surface roughness.

As noted the literature review, the effect of t_{off} on the final surface roughness is contrasting, and the reasons are unclear. The behaviour of surface roughness in the case of PBF-LB agreed with the results reported by refs. [19,20], in which conventional technologies were used to manufacture the W-EDM machined workpieces. However, the results when machining PBF-EB specimens are corroborated in several works, such as refs. [10,18,21]. For casted samples, similarly to the PBF-LB, the effect of I is almost parabolic, with a maximum at 3A, and an increase in t_{off}* was found detrimental for Ra_x. Therefore, Despite the same nominal composition, the material behaves as if it were processing different materials [25]. This result may be also explained by the fact that each production technology generates a different thermal history on the material that modifies the material microstructure and the corresponding thermal and electrical conductivities. This effect has been recently demonstrated by Altug et al. [41] when analysing the modification of material properties subjected to different heat treatments. This finding can also be supported by combining the results of Eshkabilov et al. [42] and Strumza et al. [43], which found that the thermal properties of the components are also affected by the material manufacturing technology, and the findings of Han et al. [44] and Choudhuri et al. [45], which demonstrated that the surface morphology strongly depends on the thermal properties of the material. The results presented in these works may also explain the findings of Refs. [46,47], which analysed the surface morphology and topography obtained after W-EDM of a material subjected to different heat treatments. In these works, the authors found that Ra depended on the heat treatment performed on the workpiece.

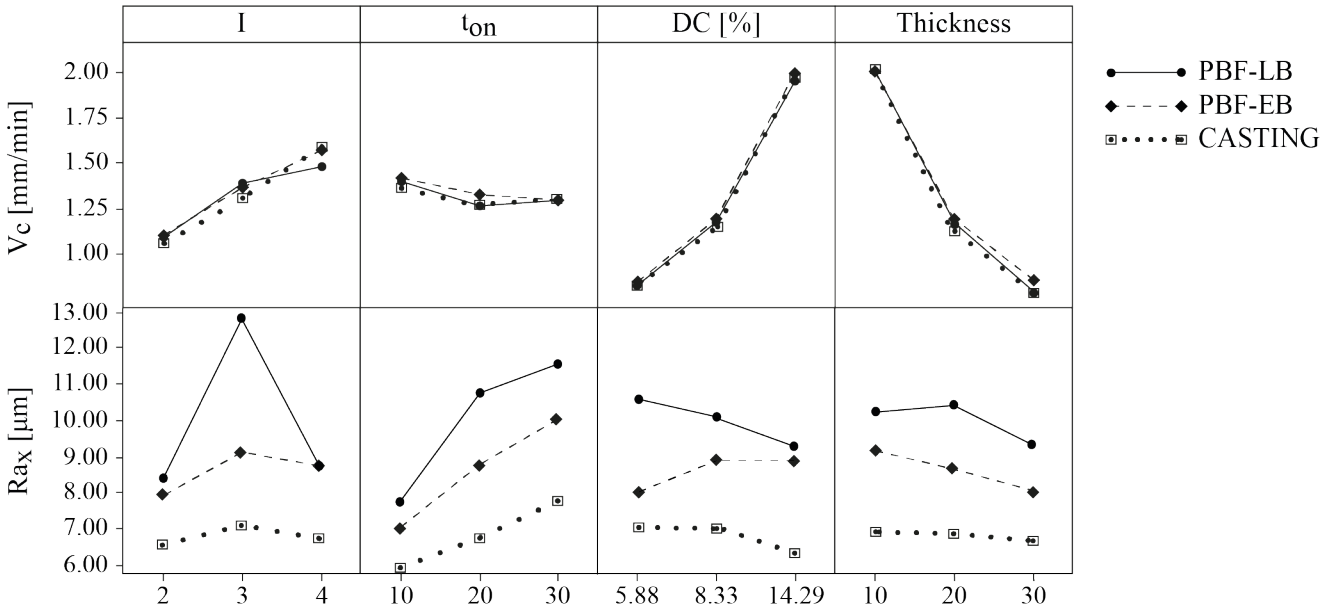

Figure 5. The main effects of process parameters on cutting speed (V_c) and Ra_x of all processes.

The cut Thickness and t_{on} variations generate almost the same effect on Ra_x for both PBF-LB and PBF-EB. The increasing t_{on} has a detrimental impact on Ra in both samples, according to refs. [7,10,12,29]. This could be explained by the fact that an increase in the discharge energy leads to larger and irregularly distributed craters that affect the surface smoothness. On the contrary, since the increased cut thickness causes a reduction in the discharge energy dispersion, Ra_x decreases, in agreement with the results of Ikram et al. [33].

To determine whether the process parameter variation significantly affects the variation of V_c and Ra_x in the case of AM parts, an ANOVA was performed with a fixed confidence level equal to 95%. Selecting a *p*-value threshold equal to 0.05, Tables 7 and 8 highlight the process parameters and their interaction, which significantly affect the V_c and Ra, respectively.

Table 7. ANOVA table of process parameters and their interactions for cutting speed V_c in the case of the PBF-LB and PBF-EB processes (significant factors or interactions are highlighted in bold).

		PBF-LB			PBF-EB		
Source	**DF**	**Adj. SS**	**Adj. MS**	***p*-Value**	**Adj. SS**	**Adj. MS**	***p*-Value**
Regression	10	43.63	4.36	0.000	41.51	4.15	0.000
I	1	0.01	0.01	0.545	0.02	0.02	0.321
t_{on}	1	0.01	0.01	0.543	0.05	0.05	0.109
DC	1	1.58	1.58	**0.000**	1.38	1.38	**0.000**
Thickness	1	5×10^{-4}	5×10^{-4}	0.911	4.3×10^{-3}	4.3×10^{-3}	0.647
I × t_{on}	1	0.01	0.01	0.558	0.04	0.04	0.173
I × DC	1	0.40	0.40	**0.003**	0.37	0.37	**0.000**
I × Thickness	1	0.22	0.22	**0.026**	0.18	0.18	**0.004**
t_{on} × DC	1	0.17	0.17	0.050	0.05	0.05	0.107
t_{on} × Thickness	1	0.16	0.16	0.059	0.08	0.08	0.050
DC × Thickness	1	2.07	2.07	**0.000**	1.89	1.89	**0.000**
Error	70	2.97	0.04		2.41	0.03	
Total	80						

Table 8. ANOVA table of process parameters and their interactions for Rax in the case of the PBF-LB and PBF-EB processes (the significant factors or interactions are highlighted in bold).

		PBF-LB			PBF-EB		
Source	**DF**	**Adj. SS**	**Adj. MS**	***p*-Value**	**Adj. SS**	**Adj. MS**	***p*-Value**
Regression	14	607.05	43.36	0.000	179.61	12.83	0.000
I	1	274.36	274.36	**0.000**	4.36	4.36	**0.029**
t_{on}	1	39.57	39.57	**0.000**	3.34	3.34	0.056
DC	1	2.92	2.92	0.162	3.95	3.95	**0.038**
Thickness	1	0.80	0.80	0.461	0.80	0.80	0.342
I × I	1	324.76	324.76	**0.000**	9.96	9.96	**0.001**
t_{on} × t_{on}	1	20.75	20.75	**0.000**	1.13	1.13	0.261
DC × DC	1	0.23	0.23	0.692	7.99	7.99	**0.003**
Thickness × Thickness	1	7.08	7.08	**0.031**	0.32	0.32	0.850
I × t_{on}	1	0.45	0.45	0.580	0.95	0.95	0.301
I × DC	1	0.95	0.95	0.421	6.64	6.64	**0.008**
I × Thickness	1	0.00	0.00	0.984	1.06	1.06	0.276
t_{on} × DC	1	1.4	1.4	0.330	0.19	0.19	0.647
t_{on} × Thickness	1	2.00	2.00	0.245	0.00	0.00	0.998
DC × Thickness	1	16.37	16.37	**0.001**	0.17	0.17	0.659
Error	66	95.97	1.45		58.00	0.87	
Total	80						

For the cutting speed (Table 7), the most significant process parameters are the same for all processes, which confirms the results of Figure 5. The most influential parameter is DC, while all the other process parameters were non-significant. The interactions between I and DC, and I and thickness, even with a total sequential sum of squares below 1%, and DC and thickness were found to be statistically significant. Further statistical tests were performed, removing the non-significant interactions. In this case, thickness and discharge current (I) also significantly affected the cutting speed, while t_{on} remained the only process parameter not to significantly affect the cutting speed. The only significant interaction was found between DC and thickness. Considering these findings, the regression model was determined considering only the DC, I, thickness, and the interaction between DC and thickness.

Regarding Ra_x, in the case of PBF-LB manufactured parts (Table 8), the discharge current, particularly its quadratic relationship with Ra_x, is the parameter that affects the surface roughness the most. Thickness and duty factor are non-significant parameters, but their interaction has a significant effect (*p*-value lower than 0.05). The quadratic impact of

thickness had a p-value below 0.05, but its contribution to the overall sum of squares was below 1%; therefore, it was excluded from the significant parameters.

For the sample manufactured by the PBF-EB process (Table 8), the discharge current, DC, and their quadratic relationship with Ra_x were found to be significant. Moreover, the interaction between DC and discharge current was significant for the roughness variation.

Because of the high contribution to experimental variability of some process parameters (e.g., t_{on} for PBF-EB, Table 8), additional statistical tests were performed for both PBF-LB and PBF-EB, removing the non-significant interactions. These tests showed thickness as a significant factor for both PBF-LB and PBF-EB. Additionally, t_{on} also became significant for PBF-EB. Those parameters were used in the next section to infer the regression models for Ra_x. The fact that models on surface roughness must be inferred using different inputs demonstrates the remarkable effect of the material manufacturing technologies on the final surface quality after W-EDM cuts.

Regression Models

The regression model that better fits the V_c data for the PBF-LB and PBF-EB process is presented in Equations (5) and (6), respectively.

$$V_c^{PBF-LB} = -0.364 + 0.193\ I + 0.245\ DC - 0.008\ Thickness - 0.005\ DC \times Thickness \quad (5)$$

$$R^2 = 91.27\%,\ R^2_{adj} = 90.81\% \text{ and } S = 0.23$$

$$V_c^{PBF-EB} = -0.512 + 0.233\ I + 0.243\ DC - 0.007\ Thickness - 0.005\ DC \times Thickness \quad (6)$$

$$R^2 = 94.74\%,\ R^2_{adj} = 94.47\% \text{ and } S = 0.17$$

From the remarkably high R^2_{adj} and low S values, it is possible to affirm that the adopted models well explain the experimental data. This observation is confirmed by the residual values and their distribution (Figure 6). The positive or negative sign of residuals can be explained by the experimental cutting order, which was always from the smallest to the largest thickness, and could have biased the results. Additionally, certain interactions between process parameters were observed to lead to unstable machining conditions that may have affected the V_c measurements. These instabilities were causal and mainly caused by short circuits, electrode retraction, and poor gap conditions.

Comparing the regression models of V_c determined for parts produced by different AM technologies, it is possible to notice that the difference between the two experimental models is almost negligible because it only consists of a slight variation in the regression coefficients. This fact again underlines that different production technologies do not significantly affect the W-EDM cutting speed index.

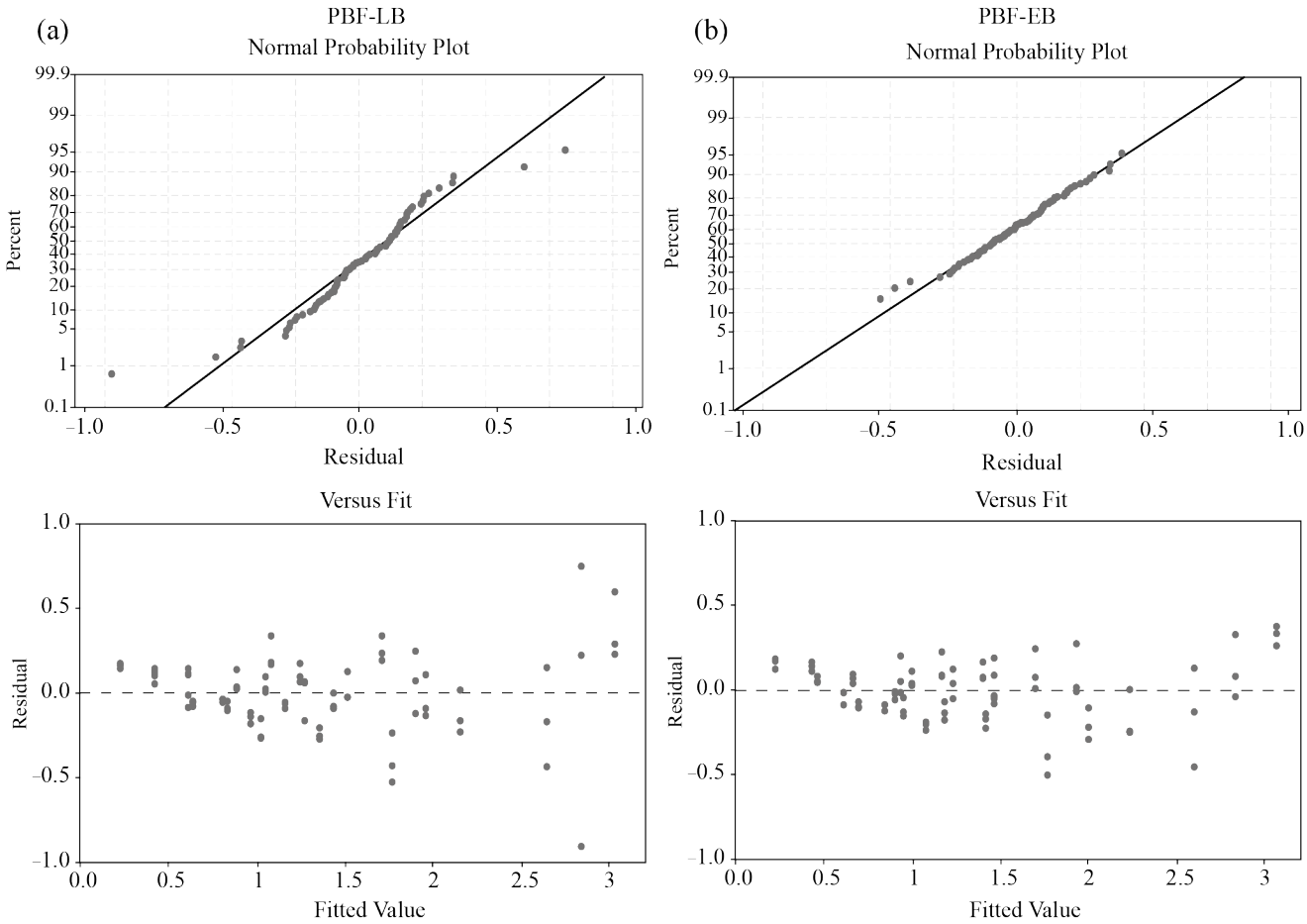

Figure 6. Residuals plots of the V_c regressions models for (**a**) PBF-LB and (**b**) PBF-EB.

The models inferred for Ra_x reflect the results of ANOVAs. The two equations are characterised by different terms and coefficients (Equations (7) and (8), for PBF-LB and PBF-EB parts, respectively.

$$\begin{aligned} Ra_x^{PBF-LB} = &-28.030 + 25.650\ I + 0.621\ t_{on} - 0.461\ DC - 0.193\ Thickness \\ &- 4.248\ I^2 - 0.010\ t_{on}^2 - 0.015\ DC\ \times\ Thickness \end{aligned} \quad (7)$$

$$R^2 = 84.62\%,\ R^2_{adj} = 83.15\% \text{ and } S = 1.22$$

$$\begin{aligned} Ra_x^{PBF-EB} = &-2.850 + 3.890\ I + 0.149\ t_{on} + 0.753\ DC - 0.056\ Thickness \\ &- 0.74\ I^2 - 0.047\ DC^2 + 0.099\ I\ \times\ DC \end{aligned} \quad (8)$$

$$R^2 = 74.10\%,\ R^2_{adj} = 71.62\% \text{ and } S = 0.92$$

The high R^2 and low S values for both models affirm that the models represent the experimental data well. This observation is confirmed by the distribution of the residuals in Figure 7, where the errors are normally distributed, and no data clustering or sign tendencies have been detected.

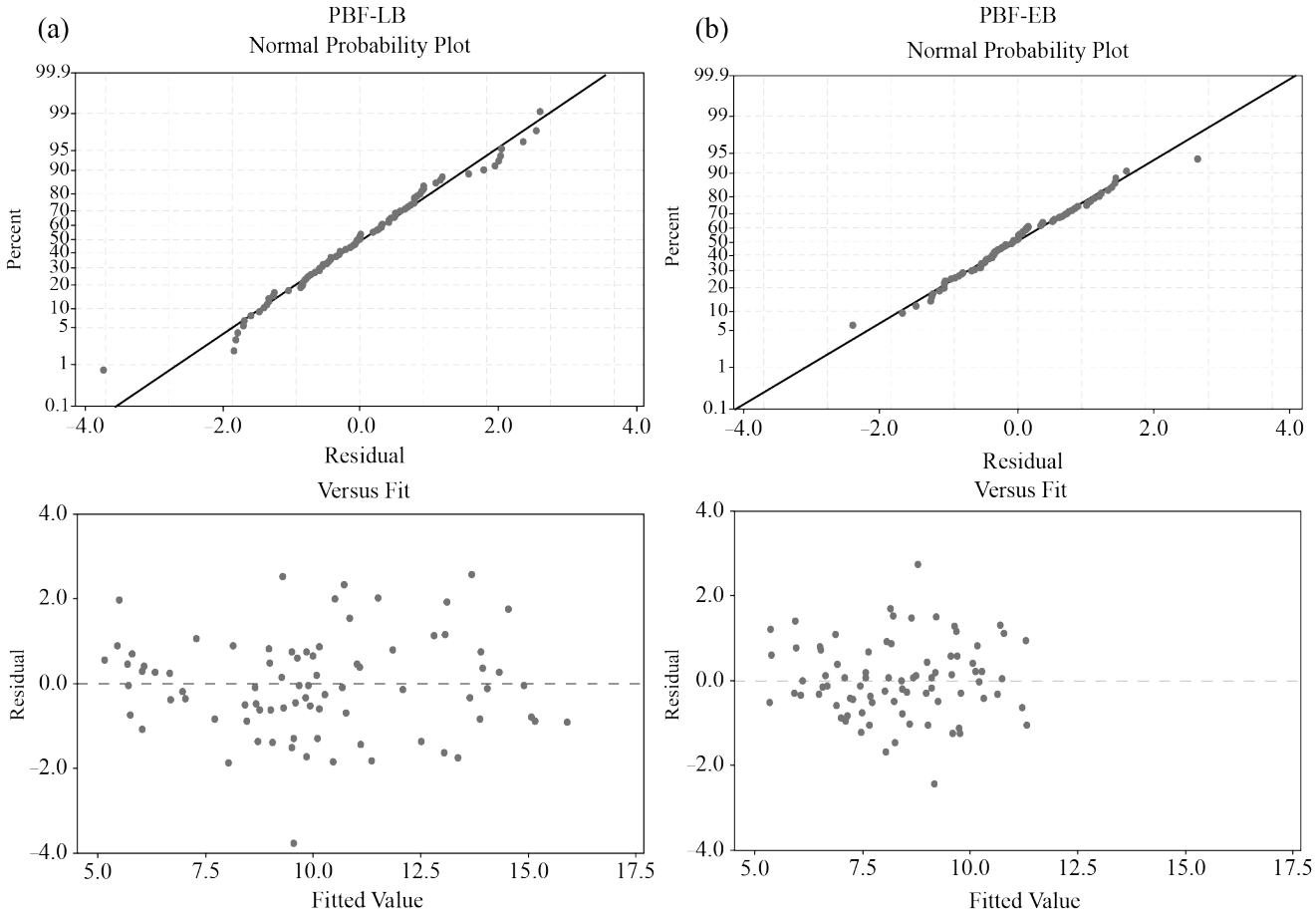

Figure 7. Residuals plots of the V_c regressions models for (**a**) PBF-LB and (**b**) PBF-EB.

4. Conclusions

This paper is the first work that investigates and compares the effect of W-EDM process parameters when processing workpieces produced by different production technologies. A full factorial experimental plan was implemented for each considered technology to test the effect of t_{on}, I, workpiece thickness, and t_{off} or DC. The material production technology strongly affected the Ra after the WED machining of samples. This was found to be particularly evident for DC and discharge current. For PBF-LB parts, increasing DC (lowering t_{off}) is beneficial for Ra_x, while it is detrimental for the PBF-EB counterpart. In both cases, Ra_x could be minimised using low I and t_{on}. These results may be explained by differences in microstructure, which may affect the electrical and thermal behaviour of the material. On the contrary, the cutting speed was not influenced by the technology. For this reason, the regression models for estimating the cutting speed for workpieces produced by different AM technologies have no significant differences. Overall, the cutting speed could be increased by adopting high I and high DC values and consequently, low t_{off} values, while larger workpiece thicknesses decreased the cutting speed.

Remarkably, the inferred models presented in this work can be used to predict the V_c and Ra values and to design specific properties for the cut surface, considering the process parameters, production technologies, and sample thickness.

Author Contributions: Conceptualization, M.G., E.A. and F.C.; methodology, M.G.; formal analysis, M.G. and P.A.; investigation, M.G. and P.A.; data curation, P.A.; writing—original draft preparation, P.A.; writing—review and editing, M.G., E.A. and F.C.; visualization, P.A.; supervision, M.G. All authors have read and agreed to the published version of the manuscript.

Funding: This research received no external funding.

Data Availability Statement: The data presented in this study are continued in the manuscript.

Acknowledgments: The authors acknowledge Elena Bassoli and Lucia Denti from Università di Modena e Reggio Emilia for providing the SEM images.

Conflicts of Interest: The authors declare that they have no known competing financial interests or personal relationships that could have appeared to influence the work reported in this paper.

Appendix A

The results of the surface roughness in the y-direction (Ra_y) for all technologies are summarised in Table 4. It is possible to notice that, as in the case of $Ra_{x,}$ there is a significant difference between the three technologies.

This is also highlighted by the ANOVA analysis (Table A1); with a risk level of 0.05, it is possible to affirm that a significant difference between the surface roughness measured in the y-direction could be found for the three different technologies (PBF-LB, PBF-EB, and casting).

Table A1. ANOVA results of the effect of all process technologies on Ra_y.

Variation Cause	DoF	Variance	F-Ratio	F-Max
Examined Factor	2	79.06	25.97	3.03
Random Errors	240	3.04		
Total	242			

Figure A1 reports the main effects of the investigated factors on Ra_y. The comparison between the three different technologies showed some differences regarding the effect of some process parameters, but there are not huge differences in the effects on the x-direction. As in the case of $Ra_{x,}$ for PBF-LB and casting, the discharge current seems to have a quadratic effect on the surface roughness along the y-direction, even if this effect is less marked in the latter case. For PBF-EB, increasing the discharge current has a detrimental effect on Ra_y, but with linear dependence. Among the three technologies, the t_{on} and thickness increase have approximately the same effect on Ra_y.

Similarly to Ra_x, t_{on} causes a surface roughness increment because the increase in the discharge energy leads to larger and more irregularly distributed craters that affect the surface smoothness. The thickness causes a surface roughness reduction due to the reduction in the discharge energy dispersion. As for Ra_x, increasing DC (reducing the t_{off} value) was found to have a detrimental effect on Ra_y for PBF-EB, while it was found to lower the surface roughness in the case of PBF-LB and casting. For all process parameter effects, the considerations made in paragraph 3 for additively manufactured and casted replicas are still valid, in this case.

Similarly to Rax, the analysis of variance (ANOVA) was performed with a fixed confidence level equal to 95% to determine which process parameters and interactions significantly affect Ra_y variation for the two AM processes. Table A2 reports all the process parameters and interactions found significant for PBF-LB and PBF-EB. In both cases, a key role is played by ton and DC, which are the two most significant factors, while the significance of the other parameters and interactions varies depending on the production technology.

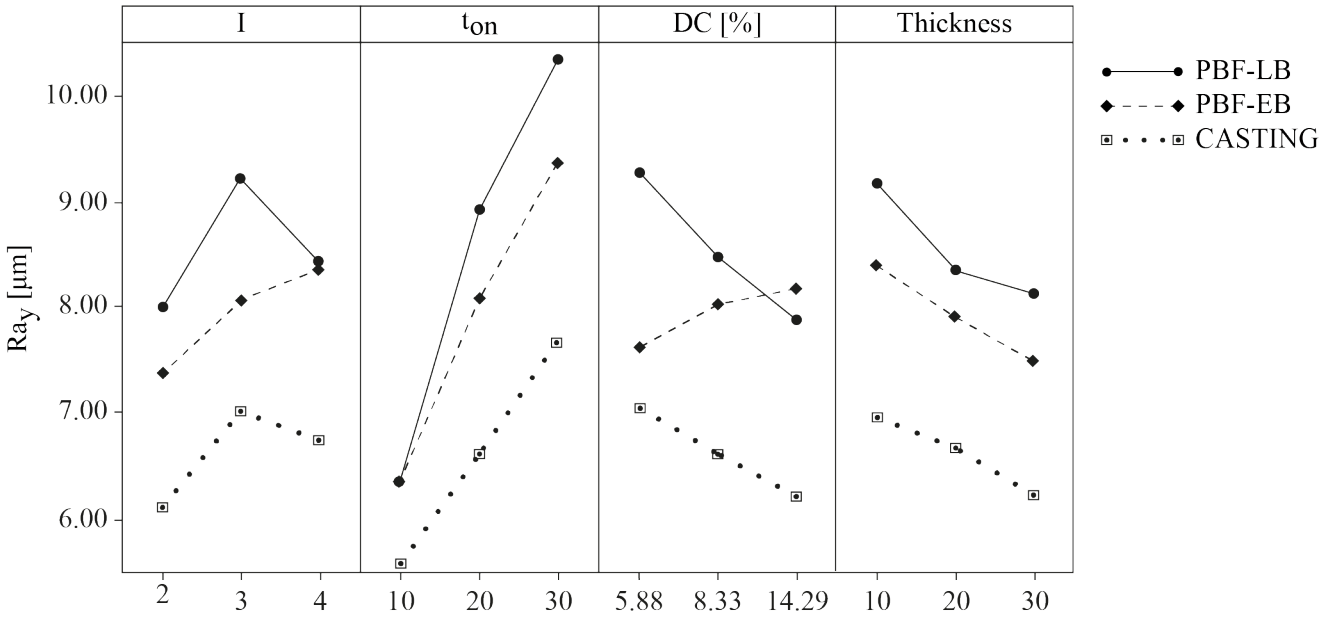

Figure A1. Main effects of process parameters Ra_y of all processes.

Table A2. ANOVA table of significant process parameters and interactions for Ra_y for PBF-LB and PBF-EB.

PBF-LB					PBF-EB				
Source	**DF**	**Adj. SS**	**Adj. MS**	***p*-Value**	**Source**	**DF**	**Adj. SS**	**Adj. MS**	***p*-Value**
Regression	6	277.20	46.20	0.000	Regression	5	168.36	33.67	0.000
I	1	18.87	18.87	0.000	I	1	7.13	7.13	0.003
t_{on}	1	20.36	20.36	0.000	t_{on}	1	123.28	123.28	0.000
DC	1	23.45	23.45	0.000	DC	1	12.71	12.71	0.000
Thickness	1	14.41	14.42	0.000	Thickness	1	11.32	11.32	0.000
I × I	1	17.76	17.75	0.000	I × DC	1	17.52	17.52	0.000
t_{on} × t_{on}	1	6.01	6.01	0.017					
Error	74	74.79	1.01		Error	75	56.29	0.75	
Total	80				Total	80			

Based on ANOVA results, two regression models, one for each additive technology, were determined as a function of the significant process parameters and interactions. In Equations (A1) and (A2), for PBF-LB and PBF-EB, respectively. In addition, R^2, R^2_{adj} and S are reported as well. According to the values and the residual values and distribution (Figure A2a,b), for which the errors are normally distributed and no data clustering or sign tendencies have been detected, it is possible to affirm that both models well explain the experimental data.

$$Ra_y^{PBF-LB} = -3.780 + 6.170\ I + 0.430\ t_{on} - 0.153\ DC - 0.052\ Thickness - 0.993\ I^2 - 0.993\ t_{on}^2 \quad (A1)$$

$$R^2 = 78.75\%,\ R^2_{adj} = 77.03\% \text{ and } S = 1.00$$

$$Ra_y^{PBF-EB} = 8.420 - 1.043\ I + 0.151\ t_{on} - 0.428\ DC - 0.046\ Thickness - 0.161\ I \times DC \quad (A2)$$

$$R^2 = 74.94\%,\ R^2_{adj} = 73.27\% \text{ and } S = 0.86$$

The high R^2 and low S values for both models affirm that the models represent the experimental data well. This observation is confirmed by the distribution of the residuals in Figure 7, where the errors are normally distributed, and no data clustering or sign tendencies have been detected.

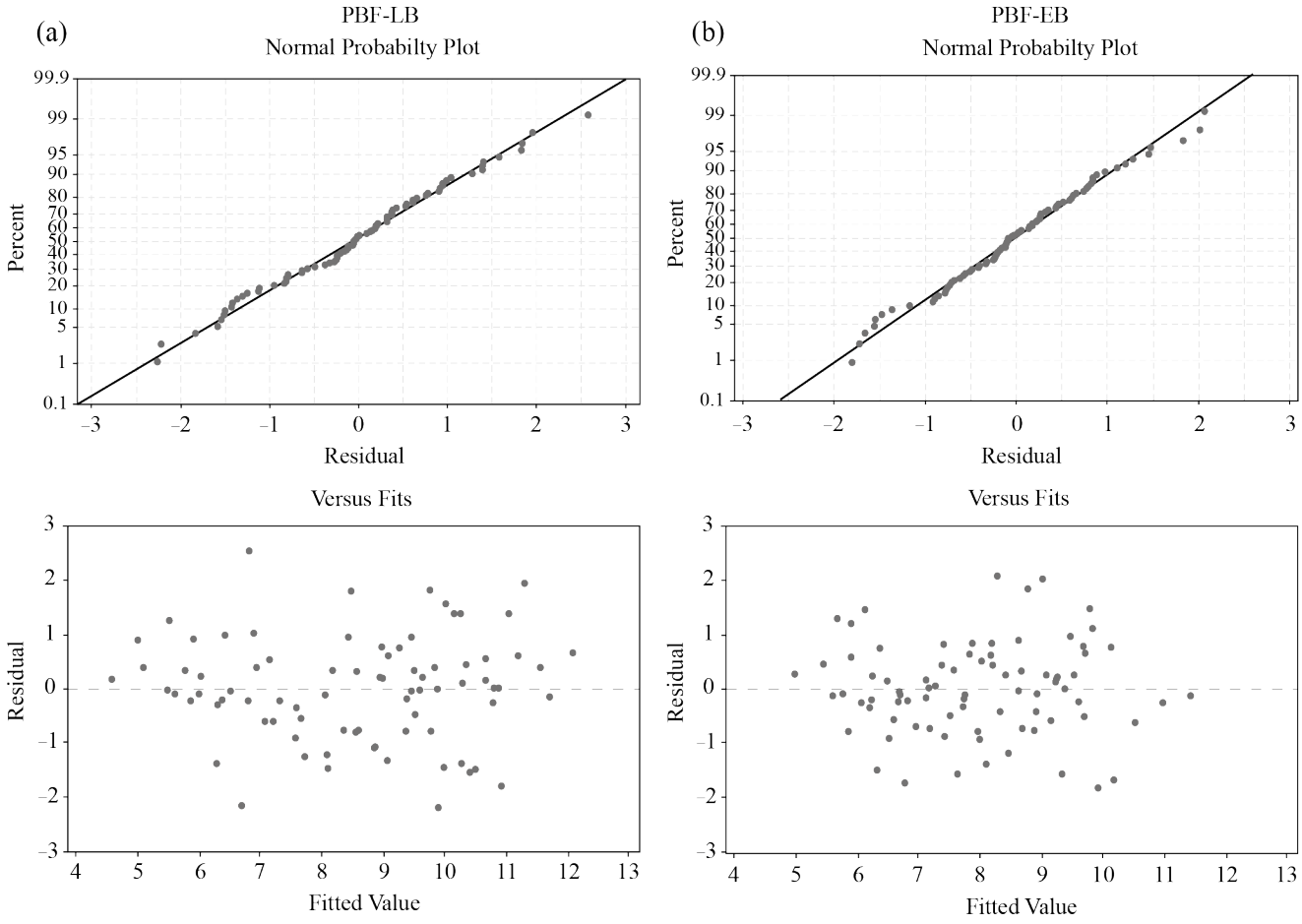

Figure A2. Residuals plots of the Ra_x regressions models for (**a**) PBF-LB and (**b**) PBF-EB.

References

1. Ho, K.H.; Newman, S.T.; Rahimifard, S.; Allen, R.D. State of the art in wire electrical discharge machining (WEDM). *Int. J. Mach. Tools Manuf.* **2004**, *44*, 1247–1259. [CrossRef]
2. Kunieda, M.; Lauwers, B.; Rajurkar, K.P.; Schumacher, B.M. Advancing EDM through Fundamental Insight into the Process. *CIRP Ann.* **2005**, *54*, 64–87. [CrossRef]
3. Garg, R.K.; Singh, K.K.; Sachdeva, A.; Sharma, V.S.; Ojha, K.; Singh, S. Review of research work in sinking EDM and WEDM on metal matrix composite materials. *Int. J. Adv. Manuf. Technol.* **2010**, *50*, 611–624. [CrossRef]
4. Defanti, S.; Denti, L.; Vincenzi, N.; Gatto, A. Preliminary assessment of electro-chemical machining for aluminum parts produced by laser-based powder bed fusion. *Smart Sustain. Manuf. Syst.* **2020**, *4*, 121–134. [CrossRef]
5. Abhilash, P.M.; Chakradhar, D. Sustainability improvement of WEDM process by analysing and classifying wire rupture using kernel-based naive Bayes classifier. *J. Braz. Soc. Mech. Sci. Eng.* **2021**, *43*, 1–9. [CrossRef]
6. Rao, P.S.; Ramji, K.; Satyanarayana, B. Experimental Investigation and Optimization of Wire EDM Parameters for Surface Roughness, MRR and White Layer in Machining of Aluminium Alloy. *Procedia Mater. Sci.* **2014**, *5*, 2197–2206. [CrossRef]
7. Kumar, A.; Kumar, V.; Kumar, J. Multi-response optimization of process parameters based on response surface methodology for pure titanium using WEDM process. *Int. J. Adv. Manuf. Technol.* **2013**, *68*, 2645–2668. [CrossRef]
8. Ghodsiyeh, D.; Lahiji, M.A.; Ghanbari, M.; Shirdar, M.R.; Golshan, A. Optimizing material removal rate (MRR) in WEDMing titanium alloy (Ti6Al4V) using the taguchi method. *Res. J. Appl. Sci. Eng. Technol.* **2012**, *4*, 3154–3161.
9. Tosun, N.; Cogun, C.; Inan, A. The effect of cutting parameters on workpiece surface roughness in wire EDM. *Mach. Sci. Technol.* **2003**, *7*, 209–219. [CrossRef]
10. Dabade, U.A.; Karidkar, S.S. Analysis of Response Variables in WEDM of Inconel 718 Using Taguchi Technique. *Procedia Cirp* **2016**, *41*, 886–891. [CrossRef]

11. Venkatarao, K.; Anup Kumar, T. An experimental parametric analysis on performance characteristics in wire electric discharge machining of Inconel 718. *Proc. Inst. Mech. Eng. Part C J. Mech. Eng. Sci.* **2019**, *14*, 4836–4849. [CrossRef]
12. Rao, K.V.; Raju, L.R.; Kumar, C.K. Modeling of kerf width and surface roughness in wire cut electric discharge machining of Ti-6Al-4V. *Proc. Inst. Mech. Eng. Part E J. Process. Mech. Eng.* **2020**, *234*, 533–542. [CrossRef]
13. Nain, S.S.; Garg, D.; Kumar, S. Evaluation and analysis of cutting speed, wire wear ratio, and dimensional deviation of wire electric discharge machining of super alloy Udimet-L605 using support vector machine and grey relational analysis. *Adv. Manuf.* **2018**, *6*, 225–246. [CrossRef]
14. Devarajaiah, D.; Muthumari, C. Evaluation of power consumption and MRR in WEDM of Ti–6Al–4V alloy and its simultaneous optimization for sustainable production. *J. Braz. Soc. Mech. Sci. Eng.* **2018**, *40*, 1–18. [CrossRef]
15. Singh, T.; Misra, J.P.; Singh, B. Experimental Investigation of Influence of Process Parameters on MRR during WEDM of Al6063 alloy. *Mater. Today Proc.* **2017**, *4*, 2242–2247. [CrossRef]
16. Singh, H.; Garg, R. Effects of process parameters on material removal rate in WEDM. *J. Achiev. Mater. Manuf. Eng.* **2009**, *32*, 70–74.
17. Sharma, N.; Khanna, R.; Gupta, R. Multi Quality Characteristics of WEDM Process Parameters with RSM. *Procedia Eng.* **2013**, *64*, 710–719. [CrossRef]
18. Chalisgaonkar, R.; Kumar, J. Optimization of WEDM process of pure titanium with multiple performance characteristics using Taguchi's DOE approach and utility concept. *Front. Mech. Eng.* **2013**, *8*, 201–214. [CrossRef]
19. Poros, D.; Wisniewska, M.; Zaborski, S. Comparative analysis of wedm with different wire electrodes applied to cut titanium ti6al4v. *J. Mach. Eng.* **2020**, *20*, 116–125. [CrossRef]
20. Priyankara, K.P.M.; Perera, G.I.P. Experimental Investigation to Achieve Minimum Surface Roughness in Wire EDM Process. In *ICSBE 2018: Proceedings of the 9th International Conference on Sustainable Built Environment*; Springer: Singapore, 2020; pp. 239–251.
21. Sharma, P.; Chakradhar, D.; Narendranath, S. Evaluation of WEDM performance characteristics of Inconel 706 for turbine disk application. *Mater. Des.* **2015**, *88*, 558–566. [CrossRef]
22. Kumar, A.; Kumar, V.; Kumar, J. Experimental investigation on material transfer mechanism in wedm of pure titanium (Grade-2). *Adv. Mater. Sci. Eng.* **2013**, *2013*, 847876. [CrossRef]
23. kumar, S.; Khan, M.A.; Muralidharan, B. Processing of titanium-based human implant material using wire EDM. *Mater. Manuf. Process.* **2019**, *34*, 695–700. [CrossRef]
24. Sen, R.; Choudhuri, B.; Barma, J.D.; Chakraborti, P. Study the impact of process parameters and electrode material on wire electric discharge machining performances. *Mater. Today Proc.* **2018**, *5*, 7552–7560. [CrossRef]
25. Calvo, R.; Daniel, M. Wire electrical discharge machining (EDM) setup parameters influence in functional surface roughness. *Procedia Manuf.* **2019**, *41*, 602–609. [CrossRef]
26. Durairaj, M.; Sudharsun, D.; Swamynathan, N. Analysis of process parameters in wire EDM with stainless steel using single objective Taguchi method and multi objective grey relational grade. *Procedia Eng.* **2013**, *64*, 868–877. [CrossRef]
27. Tosun, N.; Cogun, C.; Tosun, G. A study on kerf and material removal rate in wire electrical discharge machining based on Taguchi method. *J. Mater. Process. Technol.* **2004**, *152*, 316–322. [CrossRef]
28. Mahapatra, S.S.; Patnaik, A. Optimization of wire electrical discharge machining (WEDM) process parameters using Taguchi method. *Int. J. Adv. Manuf. Technol.* **2007**, *34*, 911–925. [CrossRef]
29. Tosun, N. The effect of the cutting parameters on performance of WEDM. *KSME Int. J.* **2003**, *17*, 816–824. [CrossRef]
30. Kumar, A.; Kumar, U.A.; Laxminarayana, P. Optimization of surface roughness and kerf width by wire cut-electrical discharge machining on inconel 625. *Mater. Today Proc.* **2020**, *27*, 1460–1465. [CrossRef]
31. Gamage, J.R.; DeSilva, A.K.M.; Chantzis, D.; Antar, M. Sustainable machining: Process energy optimisation of wire electrodischarge machining of Inconel and titanium superalloys. *J. Clean Prod.* **2017**, *164*, 642–651. [CrossRef]
32. Kumar, A.; Kumar, V.; Kumar, J. Parametric Effect on Wire Breakage Frequency and Surface Topography in WEDM of Pure Titanium. *J. Mech. Eng. Technol.* **2013**, *1*, 51–56. [CrossRef]
33. Ikram, A.; Mufti, N.A.; Saleem, M.Q.; Khan, A.R. Parametric optimization for surface roughness, kerf and MRR in wire electrical discharge machining (WEDM) using Taguchi design of experiment. *J. Mech. Sci. Technol.* **2013**, *27*, 2133–2141. [CrossRef]
34. Vaidyaa, P.; John, J.J.; Puviyarasan, M.; Prabhu, T.R.; Prasad, N.E. Wire EDM Parameter Optimization of AlSi10Mg Alloy. *Trans. Indian Inst. Met.* **2021**, *74*, 2869–2885. [CrossRef]
35. Franczyk, E.; Machno, M.; Zębala, W. Investigation and optimization of the slm and wedm processes' parameters for the AlSi10Mg-sintered part. *Materials* **2021**, *14*, 410. [CrossRef] [PubMed]
36. Calignano, F.; Manfredi, D.; Ambrosio, E.P.; Biamino, S.; Pavese, M.; Fino, P. Direct fabrication of joints based on direct metal laser sintering in aluminum and titanium alloys. *Procedia CIRP* **2014**, *21*, 129–132. [CrossRef]
37. Galati, M.; Rizza, G.; Defanti, S.; Denti, L. Surface roughness prediction model for Electron Beam Melting (EBM) processing Ti6Al4V. *Precis. Eng.* **2021**, *69*, 19–28. [CrossRef]
38. Kumar, S.; Singh, R.; Singh, T.P.; Sethi, B.L. Surface modification by electrical discharge machining: A review. *J. Mater. Process. Technol.* **2009**, *209*, 3675–3687. [CrossRef]
39. *ISO 4288*; 1996-Geometrical Product Specifications (GPS)—Surface Texture: Profile Method—Rules and Procedures for the Assessment of Surface Texture. International Organization for Standardization: Geneva, Switzerland, 1996.
40. Calignano, F. Investigation of the accuracy and roughness in the laser powder bed fusion process. *Virtual Phys. Prototyp.* **2018**, *13*, 97–104. [CrossRef]

41. Altug, M.; Erdem, M.; Ozay, C. Experimental investigation of kerf of Ti6Al4V exposed to different heat treatment processes in WEDM and optimization of parameters using genetic algorithm. *Int. J. Adv. Manuf. Technol.* **2015**, *78*, 1573–1583. [CrossRef]
42. Eshkabilov, S.; Ara, I.; Sevostianov, I.; Azarmi, F.; Tangpong, X. Mechanical and thermal properties of stainless steel parts, manufactured by various technologies, in relation to their microstructure. *Int. J. Eng. Sci.* **2021**, *159*, 103398. [CrossRef]
43. Strumza, E.; Yeheskel, O.; Hayun, S. The effect of texture on the anisotropy of thermophysical properties of additively manufactured AlSi10Mg. *Addit. Manuf.* **2019**, *29*, 100762. [CrossRef]
44. Han, F.; Jiang, J.; Yu, D. Influence of machining parameters on surface roughness in finish cut of WEDM. *Int. J. Adv. Manuf. Technol.* **2007**, *34*, 538–546. [CrossRef]
45. Choudhuri, B.; Sen, R.; Ghosh, S.K.; Saha, S.C. Comparative machinability characterization of wire electrical discharge machining on different specialized AISI steels. *Bull. Mater. Sci.* **2020**, *43*, 1–12. [CrossRef]
46. Mouralova, K.; Kovar, J.; Klakurkova, L.; Blazik, P.; Kalivoda, M.; Kousal, P. Analysis of surface and subsurface layers after WEDM for Ti-6Al-4V with heat treatment. *Measurement* **2018**, *116*, 556–564. [CrossRef]
47. Mouralova, K.; Kovar, J.; Klakurkova, L.; Prokes, T.; Horynova, M. Comparison of morphology and topography of surfaces of WEDM machined structural materials. *Measurement* **2017**, *104*, 12–20. [CrossRef]